Chapter 13

Modeling of Inlet, Exhaust, and Pipe Systems

13.1 Unified Modular Treatment

This chapter deals with the numerical modeling of the components pertaining to group 1 discussed in section 13.1.1. The components pertaining to this category are the connecting pipes, inlet and exhaust systems, as shown in Figure 13.1.

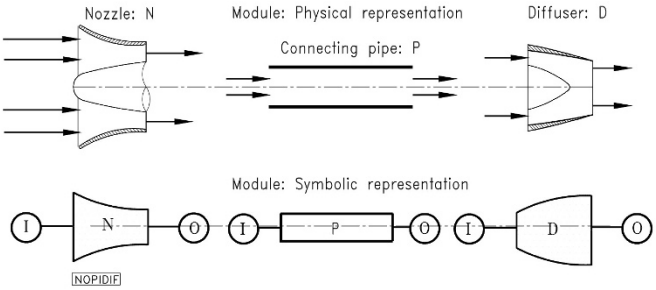

Figure 13.1: Component and modular representation of inlet nozzle N, connecting pipe P, and Diffuser D.

The function of this group consists, among other things, of the transportation of mass flow, and of converting the kinetic energy into potential energy and vice versa. Their geometry differs only in the sign of the gradient of the cross section in streamwise direction $\partial S/\partial x$. For $\partial S/\partial x < 0$, flow is accelerated for subsonic and decelerated for supersonic Mach numbers. On the other hand, for $\partial S/\partial x > 0$, the flow is decelerated for subsonic and accelerated for supersonic Mach numbers.

M. T. Schobeiri, *Gas Turbine Design, Components and System Design Integration*, https://doi.org/10.1007/978-3-030-23973-2_13

13.2 Physical and Mathematical Modeling of Modules

For modeling ducts with the varying cross sections, we apply the conservation laws derived in Chapter 11 ([1], [2], [3], [4]). The temporal change of the density at position k, shown in Figure 13.2, is determined from (11.26) as is given below:

$$\frac{\partial \rho_k}{\partial t} = -\frac{1}{\Delta x}\left(\frac{\dot{m}_{i+1}}{S_{i+1}} - \frac{\dot{m}_i}{S_i}\right). \tag{13.1}$$

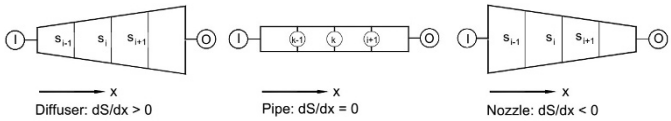

Figure 13.2: Modeling the components diffuser $\partial S/\partial x > 0$, pip $\partial S/\partial x = 0$ and nozzle $\partial S/\partial x < 0$.

The mass flows $\dot{m}_i$ and $\dot{m}_{i+1}$ at stations i and $i+1$ are determined in conjunction with the momentum equation (11.33):

$$\begin{aligned}\frac{\partial \dot{m}_k}{\partial t} = &-\frac{1}{\Delta x}(\dot{m}_{i+1}V_{i+1} - \dot{m}_i V_i + p_{i+1}S_{i+1} - p_i S_i) \\ &+ \left(\frac{\dot{m}_k V_k + P_k S_k}{S_k}\right)\left(\frac{S_{i+1} - S_i}{\Delta x}\right) - c_f \frac{\dot{m}_k^2}{2D_{h_k}\rho_k S_k}.\end{aligned} \tag{13.2}$$

The energy equation in terms of total pressure Equation (11.54) in the absence of heat addition is modified as follows:

$$\begin{aligned}\frac{\partial P_k}{\partial t} = &-\frac{\kappa_k}{\Delta x}\left(\frac{\dot{m}_{i+1}p_{i+1}}{\rho_{i+1}S_{i+1}} - \frac{\dot{m}_i p_i}{\rho_i S_i}\right) - (\kappa_k - 1)\left(\frac{\dot{m}_k q_k}{\Delta V} + c_{f_k}\frac{\dot{m}_{i+1}\dot{m}_k^2}{2D_{h_{i+1}}S_{i+1}\rho_k^2}\right) \\ &- (\kappa_k - 2)\frac{\dot{m}_k}{\rho_k S_k^2}\left[\frac{1}{2}\frac{\dot{m}_k}{\rho_k}\frac{1}{\Delta x}\left(\frac{\dot{m}_{i+1}}{S_{i+1}} - \frac{\dot{m}_i}{S_i}\right) + \frac{\partial \dot{m}_{i+1}}{\partial t}\right] \\ &- \frac{(\kappa_k - 2)}{2\Delta x}\left(\frac{\dot{m}_{i+1}^3}{\rho_{i+1}^2 S_{i+1}^3} - \frac{\dot{m}_i^3}{\rho_i^2 S_i^3}\right).\end{aligned} \tag{13.3}$$

For a constant cross-section, the equation of continuity equation (13.1) and motion equation (13.2) are written respectively as:

$$\frac{\partial \rho}{\partial t} = -\frac{1}{\Delta x S}(\dot{m}_{i+1} - \dot{m}_i) \tag{13.4}$$

$$\frac{\partial \dot{m}_k}{\partial t} = -\frac{1}{\Delta x}\left[\frac{\dot{m}_{i+1}^2}{\rho_{i+1}S} - \frac{\dot{m}_i^2}{\rho_i S} + S(P_{i+1} - P_1)\right] - c_f \frac{\dot{m}_k^2}{2\rho_k S D_h}. \tag{13.5}$$

Similarly, the equation of energy in terms of total pressure is simplified to:

$$\frac{\partial P_k}{\partial t} = -\frac{\kappa_k}{\Delta x S}\left(\frac{\dot{m}_{i+1}p_{i+1}}{\rho_{i+1}} - \frac{\dot{m}_i p_i}{\rho_i}\right) - (\kappa_k - 1)\left(\frac{\dot{m}_k q_k}{\Delta V} + c_{f_k}\frac{\dot{m}_{i+1}\dot{m}_k^2}{2D_{h_{i+1}}\rho_k^2 S^3}\right)$$
$$- (\kappa_k - 2)\frac{\dot{m}_k}{\rho_k S^2}\left[\frac{1}{2}\frac{\dot{m}_k}{\rho_k}\frac{1}{\Delta x S}(\dot{m}_{i+1} - \dot{m}_i) + \frac{\partial \dot{m}_{i+1}}{\partial t}\right]$$
$$- \frac{(\kappa_k - 2)}{2\Delta x S^3}\left(\frac{\dot{m}_{i+1}^3}{\rho_{i+1}^2} - \frac{\dot{m}_i^3}{\rho_i^2}\right). \tag{13.6}$$

Equations (13.4), (13.5), and (13.6) describe the transient process of a compressible flow within a tube with a constant cross section. For an incompressible flow (13.5) can be reduced to a simple differential equation:

$$\frac{\partial \dot{m}}{\partial t} = \frac{R\dot{m}^2}{LS}\left(\frac{T_1}{P_1} - \frac{T_n}{P_n}\right) + \frac{S}{L}(P_1 - P_n) - c_f\frac{\dot{m}^2}{\rho S D_h}. \tag{13.7}$$

The friction coefficient c_f can be determined from the known steady-state condition, where the temporal changes of the mass flow are set equal to zero. The indices 1 and n refer to the first and last station of the component. The solution of Equations (13.1)-(13.2), and Equations (13.4)-(13.7) can be performed using the implicit integration method discussed later. However, considerable calculation speed is reached if the component under investigation is subdivided into several subsections that are connected to each other via plena. In this case, for each discrete section, the mass flow can be considered as spatially independent, which leads to further simplification of the above equations.

13.3 Example: Dynamic behavior of a Shock Tube

Simulation of a high frequency compression-expansion process within a shock tube is an appropriate example to demonstrate the nonlinear dynamic behavior of the above components. The shock-expansion process within shock tubes has been the subject of classical gas dynamics for many decades ([5], [6], [7], [8]). With the introduction of fast response surface mounted sensors, shock tubes have gained practical relevance for calibrating the high frequency response pressure and temperature probes. In classical gas dynamics, shock-expansion process are treated using the method of characteristics. Results of studies presented in [9] show substantial disagreement between calculations using method of characteristics and experiments. In this and the subsequent chapters, we simulate the dynamic behavior of each individual component using the simulation code GETRAN [2]. In GETRAN, the system of non-linear differential equations is solved using the implicit solution method described in Chapter 12.

The shock tube under investigation has a length of $L = 1m$ and a constant diameter $D = 0.5m$. The tube is divided into two equal length compartments separated by a membrane. The left compartment has a pressure of $p_L = 100$bar, while the right one has a pressure of $p_R = 50$bar. Both compartments are under the same temperature of $T_L = T_R = 400K$. The working medium is dry air, whose thermodynamic properties, specific heat capacities, absolute viscosity, and other substance quantities change during the process and are calculated using a gas table integrated in GETRAN. The pressure ratio of 2 to 1 is greater than the critical pressure ratio and allows a shock propagation with the speed of sound. Two equivalent schemes can be used to predict the compression-expansion process through the tube. These are shown in Figure 13.3. In schematic (a), each half of the tube is subdivided into 10 equal pieces. The corresponding coupling plane 1 though 11, and thus, the left half of the tube are under pressure of 100 bar, while the right half with the plenums 12 through 21 are under the pressure of 50 bar.

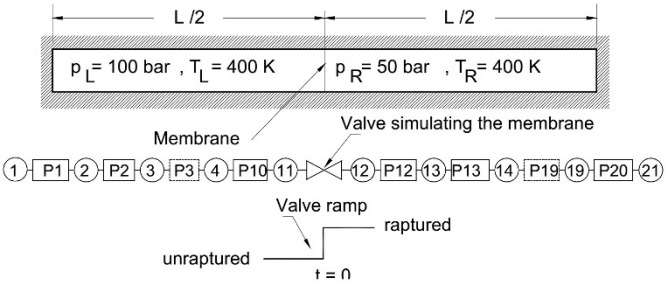

Figure 13.3: Simulation schematics for a shock tube: the physical tube (top), and the simulation schematics (a) and (b).

The membrane is modeled by a throttle system with a ramp that indicates the cross sectional area shown underneath the throttle. The sudden rupture of the membrane is modeled by a sudden jump of the ramp. The schematic (b) offers a simpler alternative. Here, as in case (a), the tube is subdivided into 20 pieces that are connected via plenums 1 to 21.

13.3.1 Shock Tube Dynamic Behavior

Pressure Transients: The process of expansion and compression is initiated by suddenly rupturing the membrane. At time $t = 0$, the membrane is ruptured which causes strong pressure, temperatures, and thus, mass flow transients. Since the dynamic process is primarily determined by pressure, temperature, and mass flow transients, only a few representative results are discussed as shown in Figures 13.4 through 13.9.

Figure 13.4 shows the pressure transients within the left sections 1 to 9. As curve 9 shows, the section of the tube that is close to the membrane reacts with a steep expansion wave. On the other hand, the pressure within the pipe section

ahead of the shock, Figure 13.5, curve 11, increases as the shock passes through the section. Oscillatory behavior is noted as the shock strength diminishes. The pipe sections that are farther away from the membrane, represented by curves 7, 5, 3, and 1 on the left and curves 13, 15, 17, and 19 on the right section, follow the pressure transient with certain time lags. Once the wave fronts have reached the end wall of the tube, they are reflected as compression waves. The aperiodic compression-expansion process is associated with a propagation speed which corresponds to the speed of sound. The expansion and compression waves cause the air, which was initially at rest, to perform an aperiodic oscillatory motion.

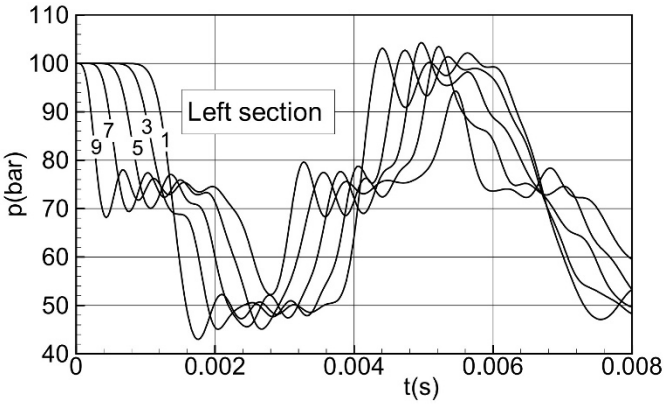

Figure 13.4: Pressure transients within the shock tube. Left section includes all tube sections initially under high pressure of 100 bar, while the right section include those initially at 50 bar.

Since the viscosity and the surface roughness effects are accounted for by introducing a friction coefficient, the transient process is of dissipative nature. This pressure rise is followed by a damped oscillating wave that hits the opposite wall and reflects back with an initially increased pressure followed by a damped oscillation

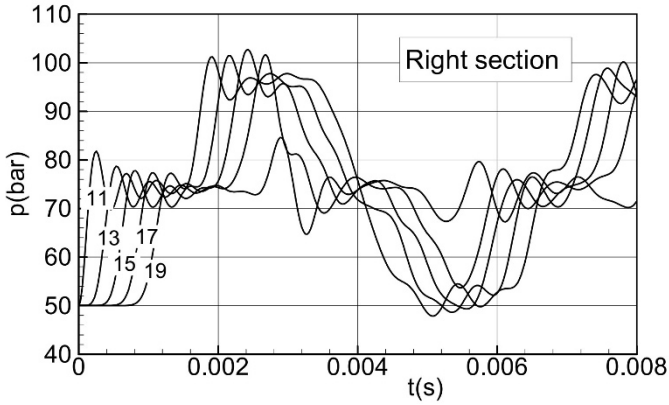

Figure 13.5: Pressure transients within the shock tube. Right section includes all tube sections initially under high pressure of 50 bar, while the left section includes those initially at 100 bar.

Temperature Transients: Figure 13.6 shows the temperature transients within the left sections 1 to 9. As curve 9 shows, the section of the tube that is close to the membrane reacts with a steep temperature decrease. The pipe sections that are farther away from the membrane, represented by curves 7, 5, 3, and 1 on the left and curves 13, 15, 17, and 19 on the right section, follow the temperature transient with certain time lags. Once the shock waves have reached the end wall of the tube, they are reflected as compression waves where the temperature experience a continuous increase.

Slightly different temperature transient behavior of the right sections are revealed in Figure 13.7. Compared to the temperature transients of the left sections, the right sections temperature transients seem to be inconsistent. However, a closer look at the pressure transients explains the physics underlying the temperature transients. For this purpose we consider the pressure transient curve 11, in Figure 13.5. The location of this pressure transient is in the vicinity of the membrane's right side with the pressure of 50 bar. Sudden rapture of the membrane simulated by a sudden ramp (Figure 13.2) has caused a steep pressure rise from 50 bar to slightly above 80 bar.

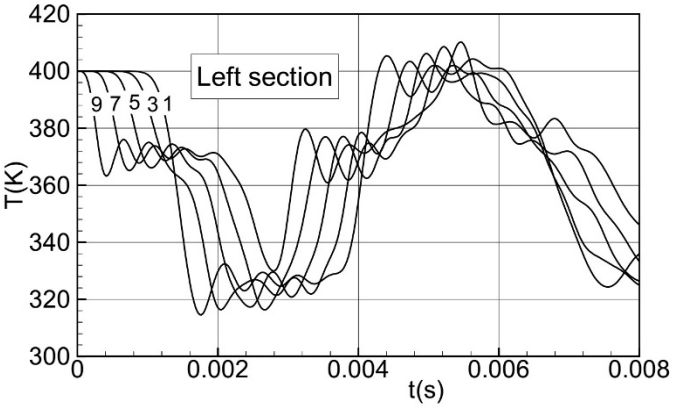

Figure 13.6: Temperature transients within the left sections of the tube. Left and right sections includes all tube sections initially under temperature of 400 K.

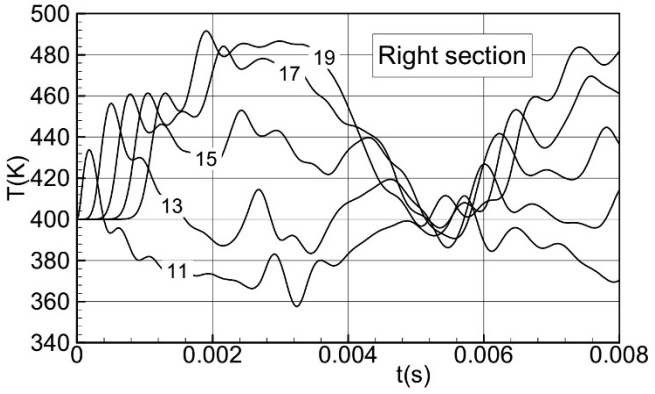

Figure 13.7: Temperature transients within the right sections of the tube. Left and right sections includes all tube sections initially under temperature of 400 K.

The pattern of the pressure transients is reflected in temperature distribution, where the pressure rise causes a temperature increase and vice versa. The temperature transients at downstream locations 12 to 20 follow the same trend.

Mass flow Transients: Figures 13.8 and 13.9 show the mass flow transients within the left and the right section of the tube. The steep negative pressure

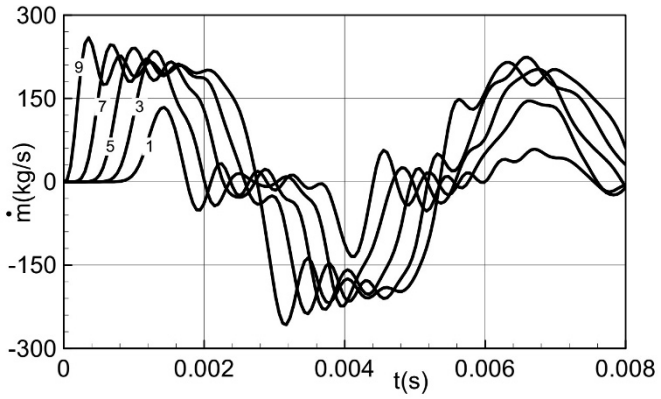

Figure 13.8: Mass flow transients within left section of shock tube.

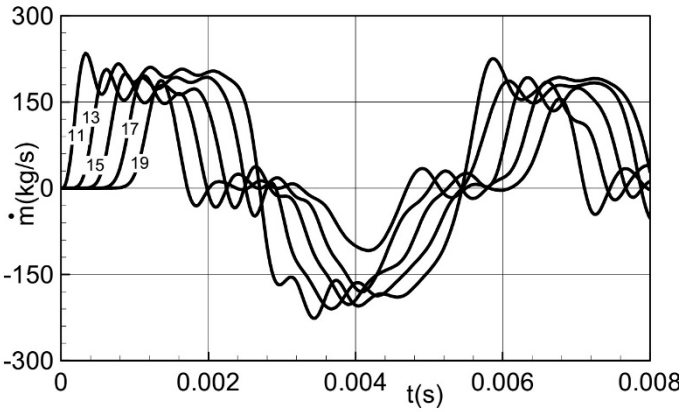

Figure 13.9: Mass flow transients within the shock tube. The right section include all tube sections initially under high pressure of 50 bar, while the left section include those initially at 100 bar.

gradient causes the mass contained within the tube to perform aperiodic oscillatory motions. During the expansion process, curve 1, mass flows in the positive x-direction. It continues to stay positive as long as the pressure in individual sections are above their minimum. This means that the shock front has not reached the right wall yet. Once the shock front hits the right wall, it is reflected initiating a compression process that causes the mass flows in the negative x-direction. Figures 13.8 through 13.9 clearly show the dissipative nature of the compression and expansion process that results in diminishing the wave amplitudes and damping the frequency. The degree of damping depends on the magnitude of the friction coefficient c_f that includes the Re-number and surface roughness effects. For a sufficiently long computational time, the oscillations of pressure, temperature, and mass flow will decay. For $c_f = 0$, the a-periodic

oscillating motion persists with no decay.

Bibliography

[1] Schobeiri T., 1986: "A General Computational Method for Simulation and Prediction of Transient Behavior of Gas Turbines," ASME-86-GT-180.

[2] Schobeiri, M. T., Abouelkheir, M., Lippke, C., 1994, "GETRAN: A Generic, Modularly Structured Computer Code for Simulation of Dynamic Behavior of Aero-and Power Generation Gas Turbine Engines," an honor paper, ASME Transactions, Journal of Gas Turbine and Power, Vol. 1, pp. 483–494.

[3] Schobeiri, M. T., Attia, M, Lippke, C., 1994, "Nonlinear Dynamic Simulation of Single and Multi-spool Core Engines, Part I: Theoretical Method," AIAA, Journal of Propulsion and Power, Volume 10, Number 6, pp. 855-862, 1994.

[4] Schobeiri, M. T., Attia, M, Lippke, C., 1994, "Nonlinear Dynamic Simulation of Single and Multi-spool Core Engines, Part II: Modeling and Simulation Cases," AIAA Journal of Propulsion and Power, Volume 10, Number 6, pp. 863–867, 1994.

[5] Prandtl, L., Oswatisch, K., Wiegarhd, K., 1984, "Führer durch die Strömung-lehre," 8. Auflage, Branschweig, Vieweg Verlag.

[6] Shapiro, A. H., 1954, "The Dynamics and Thermodynamics of Compressible Fluid Flow," Vol. I, Ronald Press Company, New York, 1954.

[7] Spurk, J, 1997, "Fluid mechanics," Springer-Verlag, Berlin, Heidelberg, New York.

[8] Becker, E., 1969, "Gasdynamik, Stuttgart," Teubner Studienbücher Mechanik, Leitfaden der angewandten Mathematik und Mechanik.

[9] Kentfield, J. A. C., 1993, "Nonsteady, One-Dimensional, Internal, Compressible Flows, Theory and Applications," Oxford University Press.